



## ENGINEERING SCIENCES

# Numerical-experimental procedure for predicting fatigue life in SAE AMS 7475-T7351 aluminum alloy considering the effect of stress ratio

MARCOS FÁBIO V. MONTEZUMA, ENIO P. DE DEUS,  
CASSIUS OLIVIO F.T. RÜCHERT, MÁRCIO C. DE CARVALHO &  
MARCELO A. E SILVA FILHO

**Abstract:** This study addresses the prediction of fatigue life in SAE AMS 7475-T7351 aluminum alloys under variable loads, commonly used in the construction of aircraft fuselages. The main objective of the research was to develop a numerical-experimental procedure to analyze crack growth, using the Walker's approach which considers the effects of the stress ratio  $R$  on the fatigue crack growth rate  $da/dN$ , combined with the Finite Element Method and Linear Regression of the Stress Intensity Factor. Observations showed that Walker's model effectively consolidated fatigue crack propagation data for various stress ratios when applied longitudinally to L-T rolling orientation, due to low dependence of exponent  $m$  on  $R$ -value in  $da/dN$  equation. Simple averaging of  $m$  values effectively calculated Walker's exponent. The methodology employed experimental tests following ASTM standards for tension, fracture toughness, and fatigue, complemented by Finite Element Method (FEM) simulations. The Walker's model proved more effective, while the Paris-Erdogan model, which ignores the  $R$  effect, resulted in overly conservative service life estimates. The principle of similitude suggests that this methodology could be effective in predicting fatigue life in cases with complex geometries, where calculating the Stress Intensity Factor Fracture parameter is challenging and the Finite Element Method shows efficiency.

**Key words:** Aluminum alloys, crack growth, fatigue failure, load ratio, numerical simulation.

## INTRODUCTION

The SAE AMS 7475-T7351 Aluminum Alloy has been designed to offer high fracture toughness and corrosion resistance, commonly used in constructing aircraft fuselages and other structures. This alloy ranks among the most mechanically robust aluminum alloys (Chemin 2012). To accurately predict the service life of materials subject to variable loads, it is essential to use equations that consider the effects of the stress ratio  $R$  on the fatigue crack growth rate  $da/dN$  (Rüchert 2007). This approach, known as damage tolerant (Fig. 1), allows for deriving fracture parameters through analytical, experimental, or computational methods.

The literature presents various expressions for fatigue crack growth rate  $da/dN$  (Bilby et al. 1963, Forman et al. 1967, Tomkins 1968, Elber 1971, Miller & Gallagher 1981, Ogura et al. 1985, Forman & Mettu

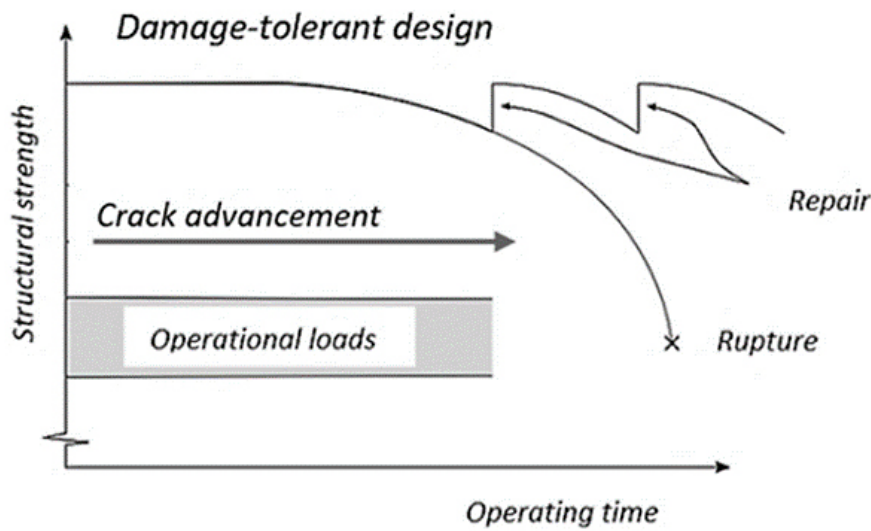


**Figure 1.** Schematic representation of the damage tolerant design approach, showing the loss of structural strength with crack progression and monitoring for repair.

1992, Chang & Hudson 1981, Bannantine et al. 1990, Lazzeri et al. 1995, Newman 1998, Decoopman 1999, Datta et al. 2018, Tong et al. 2019). Paris et al. (1961) related the variation of the Stress Intensity Factor  $\Delta K$  with  $da/dN$ . However, it was discovered that  $\Delta K$  alone could not correlate the crack growth rates at different stress ratios  $R$  (Duran & Hernandez 2015), leading to other equations. Specifically, Walker (1970) proposed an empirical relationship where an effective  $\Delta K'$  could predict the influence of the stress ratio  $R$  on  $da/dN$ .

$$\Delta K' = \frac{\Delta K}{(1 - R)^{1-\gamma_w}} \tag{1}$$

Equation (1) is known as the Walker’s equation, where  $\gamma_w$  is the Walker’s exponent assumed to be a material constant dependent on the stress ratio  $R$ , and  $\Delta K'$  is the equivalent stress intensity variation for  $R = 0$  that causes the same growth rate for a combination of  $K_{max}$  and  $R$ . It is important to note that when  $R = 0$ ,  $\Delta K'$  is equal to  $\Delta K$ . In other words, Walker’s equation consolidates the fatigue crack growth data at  $R = 0$ . Therefore, the Paris-Erdogan Equation can be modified as shown in Eq. (2):

$$\frac{da}{dN} = C_0 (\Delta K')^{m_0} = C_0 (1 - R)^{-(1-\gamma_w)m_0} (\Delta K)^{m_0} \tag{2}$$

where  $C_0$  and  $m_0$  are respectively the Paris coefficient and exponent for  $R = 0$ , noting that  $C_0 = C_{R=0}$  and  $m_0 = m_{R=0}$ . According to Rosenfeld (1997), Equations (1) and (2) can be applied in cases where the  $da/dN$  lines are parallel. Consequently, the Paris exponent  $m$  is constant ( $m = m_0$ ), regardless of the stress ratio  $R$ . In the analytical procedure proposed by Zheng and Powell (1999), small differences in  $m$  are considered by the simple average of values at different stress ratios  $R$ .

Therefore, the term  $C_0 (1 - R)^{-(1-\gamma_w)m_0}$  in Eq. (3) represents the Paris coefficient,  $C$ , for a specific stress ratio  $R$ :

$$C = C_0 (1 - R)^{-(1-\gamma_w)m_0} \tag{3}$$

Applying a logarithmic transformation to both sides:

$$\log C = \log C_0 - (1 - \gamma_w) m_0 \log(1 - R) \tag{4}$$

where  $\log C_0$  and  $-(1 - \gamma_w) m_0$  are the coefficients of the equation obtained through linear regression (LR) analysis of the graph  $\log C$  versus  $\log(1 - R)$ , thus allowing the calculation of  $\gamma_w$ . By integrating Eq. (2), it is possible to develop a mathematical expression to predict the fatigue life  $N$  of a component subjected to constant amplitude loading.

$$\int_{N_0}^N dN = \int_{a_0}^a \frac{da}{C(\Delta K)^m} = \int_{a_0}^a \frac{da}{C(Y\Delta\sigma\sqrt{\pi a})^m} = \frac{1}{C(Y\Delta\sigma\sqrt{\pi})^m} \int_{a_0}^a \frac{da}{a^{m/2}} \quad (5)$$

$$N = \frac{2 \left( a_0^{1-\frac{m}{2}} - a^{1-\frac{m}{2}} \right)}{C(m-2)(Y\Delta\sigma\sqrt{\pi})^m}, m \neq 2 \quad (6)$$

$$N = \frac{\ln\left(\frac{a}{a_0}\right)}{\pi C(Y\Delta\sigma)^2}, m = 2 \quad (7)$$

These expressions involve three variables.  $Y$  is a constant that depends on the geometry of the component being tested, while  $\Delta\sigma$  is the applied stress range.  $N$  represents the number of cycles required for a crack to grow from its initial length of  $a_0$  to its final length  $a$ . Eventually, the fracture will occur when the crack reaches a critical value of  $a_c$  and  $K_{max}$  equals to the fracture toughness  $K_C$ . The stress intensity factor (SIF) can be calculated numerically through the finite element method (FEM), which uses solutions of stress and strain fields at the crack front. This calculation employs the formulation of the interaction integral  $I_0$  during the solution phase of the analysis (Song & Paulino 2006). The interaction integral is a formula that involves two types of fields: auxiliary and actual fields. The auxiliary fields are based on previously known fields like Williams' solution (Williams 1957). The actual fields, on the other hand, use quantities like displacements, strains, and stresses that are obtained through numerical methods like FEM. The actual and auxiliary fields are superimposed on the path-independent  $J$ -integral on the interaction integral (Rice 1968).

$$I_0 = - \int_V q_{i,j} \left[ \sigma_{k,l} \varepsilon_{k,l}^{aux} \delta_{i,j} - \sigma_{k,j}^{aux} u_{k,i} - \sigma_{k,i} u_{k,j}^{aux} \right] dV / \int_S \delta q_n dS \quad (8)$$

Where,  $\sigma_{i,j}$ ,  $\varepsilon_{i,j}$ ,  $u_i$  are stress, strain, and displacement, respectively.  $\sigma_{i,j}^{aux}$ ,  $\varepsilon_{i,j}^{aux}$ ,  $u_i^{aux}$  are stress, strain, and displacement, respectively, of the auxiliary field  $q_i$  is the crack extension vector. The interaction integral is associated with the stress intensity factors as follows:

$$I = \frac{2}{E^*} (K_1 K_1^{aux} + K_2 K_2^{aux}) + \frac{1}{\mu} K_3 K_3^{aux} \quad (9)$$

where,  $K_i$  ( $i = 1,2,3$ ) = SIF in Modes I, II, and III, respectively;  $K_i^{aux}$  ( $i = 1,2,3$ ) = SIF auxiliary in Modes I, II, and III;  $E^* = E$  for a predominant plane stress state;  $E^* = E/(1 - \nu^2)$  for a predominant plane strain state;  $E$  = Young's modulus;  $\nu$  = Poisson's ratio;  $\mu$  = Shear modulus. The auxiliary fields, specified in Eq. (8) and (9), are based on local crack tip coordinate systems and represent the asymptotic stress and strain fields for crack configurations in Modes I, II, and III. The interaction integral has been used to compute Stress Intensity Factors (SIFs) using appropriate auxiliary fields that must be chosen. These fields should be defined to include the quantities to be determined, such as  $K_I$ ,  $K_{II}$ , and  $K_{III}$  (Yau et al. 1980).

The FEM is advantageous for calculating the SIF, particularly for complex geometries that differ from those used in standardized tests (Montezuma 2022, Galic et al. 2018, Zienkiewicz 1994, Yang 1986). Finite Element Method (FEM) is a technique where the system domain is divided into simpler components, and this makes it easier to obtain partial solutions, which are then combined to obtain an approximate solution to the problem. FEM allows for modeling and analyzing structures with complex shapes, which are challenging to analyze using analytical methods. The use of higher-order interpolation functions in FEM allows for an accurate representation of material and geometry behavior. This feature is handy in regions with high-stress gradients, such as at crack fronts, where precise results are required. With the advancement of digital computers and CAE programs, solving discrete problems, such as those found in FEM, has become feasible even with a large number of elements. Determining the SIF (Stress Intensity Factor) distribution in crack growth analysis is crucial for predicting the remaining component life. Thanks to the development of finite element techniques, this analysis can be performed using Linear Elastic Fracture Mechanics (LEFM). Courtin et al. (2005) has discussed the significant methods reported in the literature. However, the Ansys program employed in this study still cannot include the effect of the stress ratio  $R$  in the crack growth calculations  $da/dN$ . The main objective of this work was to present a numerical-experimental procedure for analyzing crack growth in SAE AMS 7475-T7351 aluminum alloy, loaded longitudinally (L-T). This procedure, proposed by the authors, utilizes the Walker's approach to investigate the effect of the stress ratio on the  $da/dN$  data, combining the finite element method and LR of the stress intensity factor. The numerical SIF results were adjusted to the Walker's model to reflect the effect of the stress ratio  $R$ , using experimental data from constant amplitude loads with a stress ratio of  $R = 0.8$ .

## MATERIALS AND METHODS

### Experimental procedures

The material for this study was provided by EMBRAER – Brazil and consists of a 60 mm thick SAE AMS 7475-T7351 aluminum alloy plate. A preferential microstructural orientation was observed along the L-T direction, corresponding to the rolling direction. Crack identification planes for plastically deformed plates are shown in (Fig. 2) by ASTM E399.

Compact Tension C(T) test specimens for fracture toughness and fatigue crack propagation were machined using electrical discharge machining in the L-T orientation, as schematically represented in Fig. 3.

The experimental procedures included tensile, fracture toughness, and fatigue tests, as reported by Todaro et al. (2006). Four cylindrical specimens were removed and machined according to ASTM-8M (2000) standard to obtain the monotonic tensile mechanical properties. An EMIC equipment was used for this test at room temperature, with a deformation speed of 1 mm/min until yielding and 4 mm/min until failure. The Tesc program version 1.10 was employed, where it was necessary to program the test steps in the manufacturer's specific Script language to obtain the stress vs. engineering strain curve, subsequently converted into an actual stress vs. true strain graph. This process allowed yield determination and ultimate strength, elongation, and reduction in area. The fracture toughness tests followed ASTM E1820-01, and were conducted in air and at room temperature in the L-T orientation.

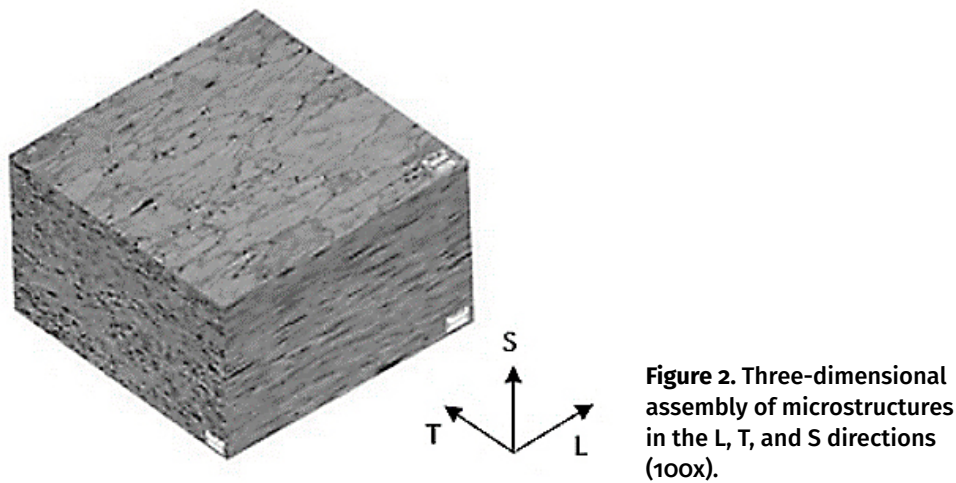


**Figure 2.** Three-dimensional assembly of microstructures in the L, T, and S directions (100x).

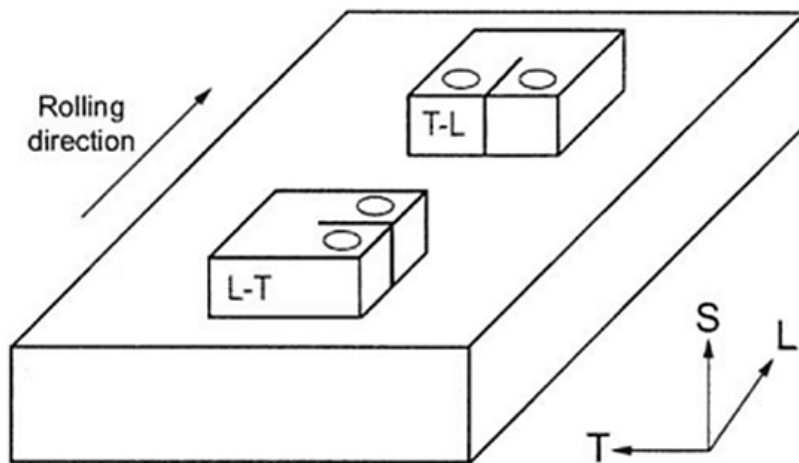


**Figure 3.** Schematic representation of specimen orientation used in fracture toughness and fatigue crack propagation tests.

The tensile tests were conducted under the same conditions, with a crosshead speed of 5 mm/min, according to ASTM E8M-00. For fatigue crack growth (FCG), the tests followed ASTM E647-00, performed in air and at room temperature, with constant load and stress ratios  $R$  of 0.1, 0.5, 0.7, and 0.8 at approximately 15 Hz. Crack growth monitoring was done using the compliance technique.

### Numerical procedures

A simulation of crack growth using the FEM was carried out using the Ansys R19 program. The SMART Crack Growth module was used, presenting an approach to simulate fatigue or static crack growth. Utilizing remeshing-based methodologies, SMART, an acronym for Separating, Morphing, Adaptive, and Remeshing Technology, automatically employs a combination of techniques to dynamically update mesh changes, enabling accurate simulation of static or fatigue crack propagation during the solution process. This module updates the mesh automatically due to crack growth at each solution step. For the simulation, on a Compact Tension C(T) specimen, with dimensions

identical to those of the specimen used in the FCG tests has been used. The dimensions of the specimen are shown in Fig. 4, considering a thickness of 25 mm.

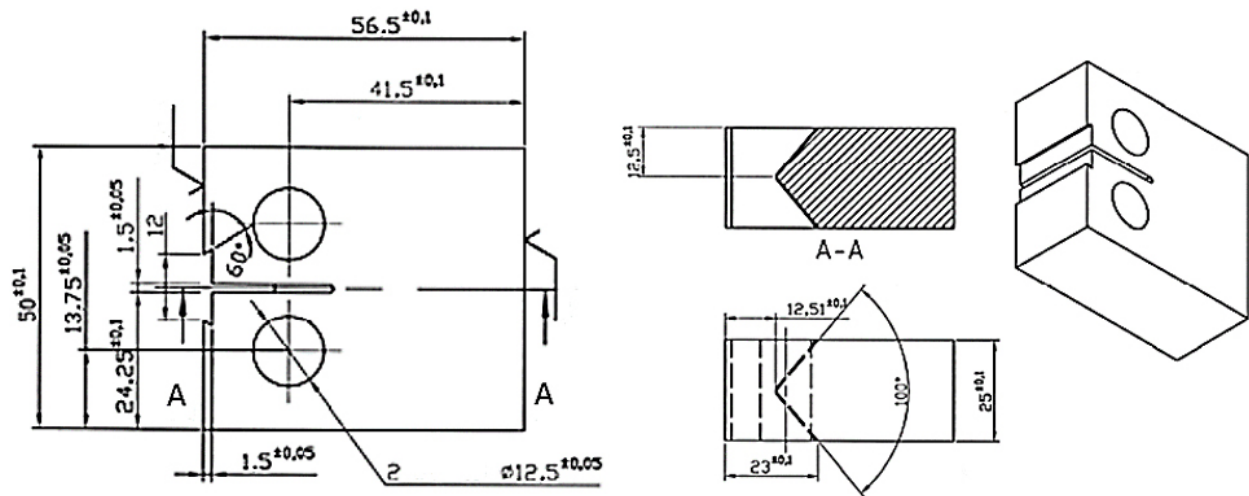


**Figure 4.** Dimensions of the Compact Tension C(T) specimen with a thickness of 25 mm.

For the simulation, fracture toughness and tensile test data were used as input (Table II). The crack propagation model employed an automatic mesh regeneration function updated at each solution step due to crack growth, adopting the critical stress intensity factor  $K_C$  as the criterion for crack advancement. A mesh refinement process and analysis of the element quality at the crack front were carried out to enhance the accuracy of fracture parameter calculations. The most critical region in a fracture model is around the crack's edge. For reliable results, the first row of elements around the crack tip should have a radius of approximately  $a/8$  or smaller (Narne et al. 2018), where  $a$  is the length of the crack. An influence sphere with a radius of 14.0 mm and an element size of 1.2 mm ( $< 20.0$  mm/8.0 mm) at the crack front was defined, and values were established after a prior mesh convergence process. 58119 elements and 81765 nodes were employed, with 85% of the elements exhibiting quality above 0.7, primarily in the region of interest at the crack tip. Fig. 5 displays only the best-quality elements; the mesh element quality is shown in Fig. 6. The type of element used was the higher-order tetrahedral SOLID187, defined by 10 nodes with three degrees of freedom at each node, consisting of translations in the  $x$ ,  $y$ , and  $z$  nodal directions. The element exhibits properties of plasticity, hyperelasticity, creep, large deflection, and large deformation capacity (Ansys 2015).

Before starting the solution, the following boundary conditions were established: restriction of three degrees of freedom at the nodes of elements on the rear face of the specimen (region C-D); application of monotonic and counteracting loads on the faces of the fixing holes A and B, as illustrated in Fig. 7.

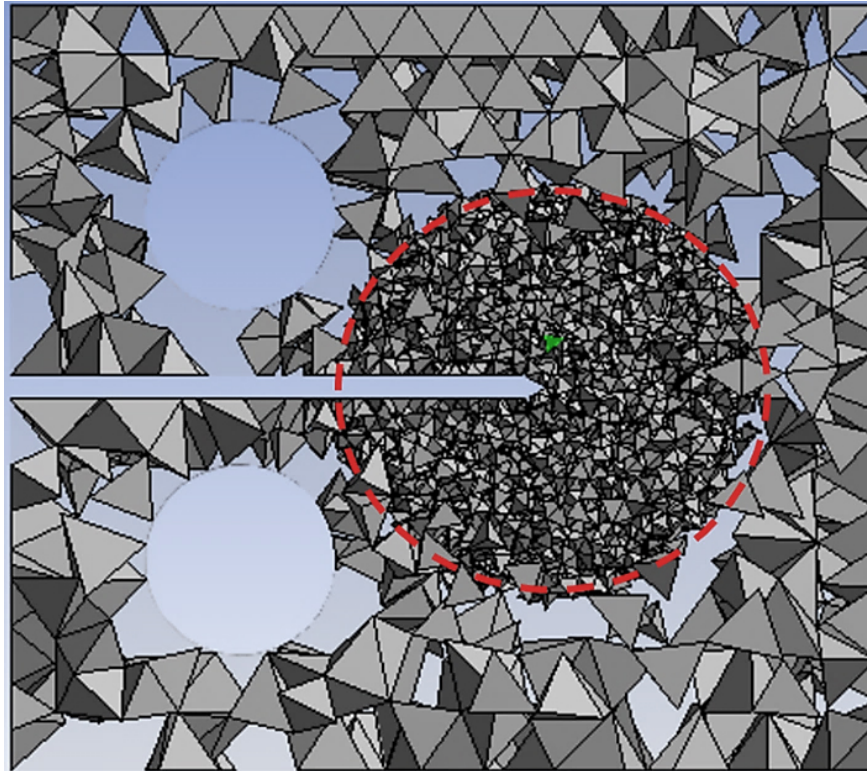


**Figure 5.** Mesh refinement at the crack front with an element size of 1.2 mm and an influence sphere of 14.0 mm (visualization of the best quality elements).

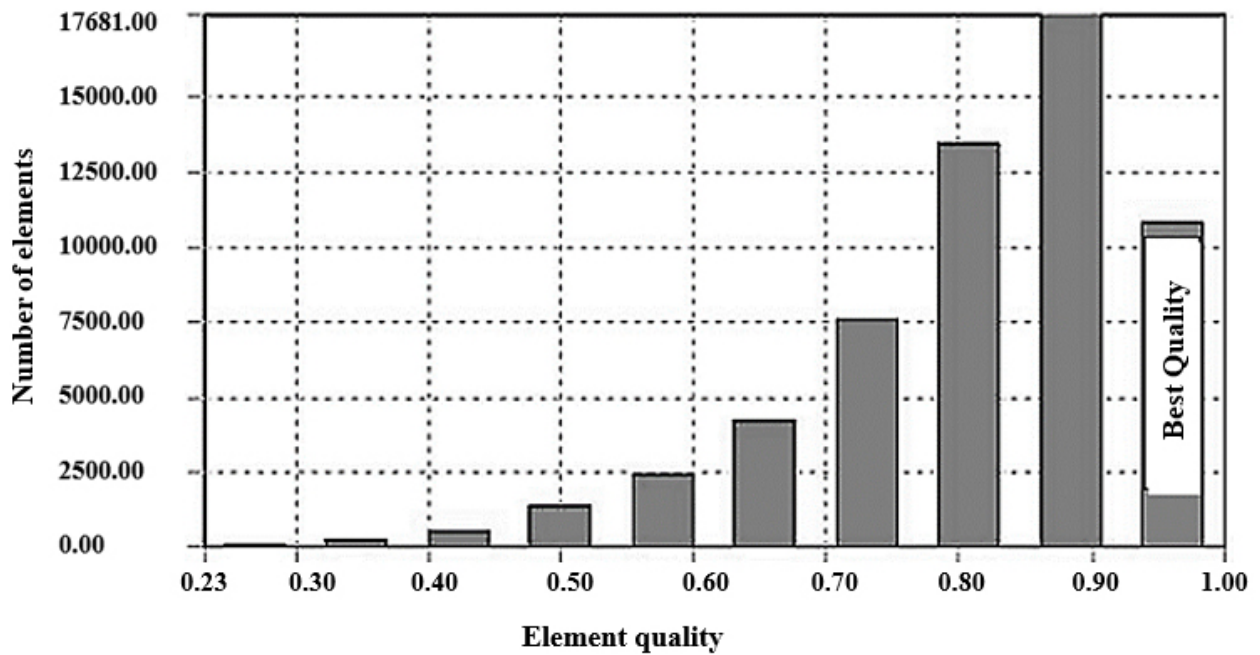


**Figure 6.** Mesh element quality.

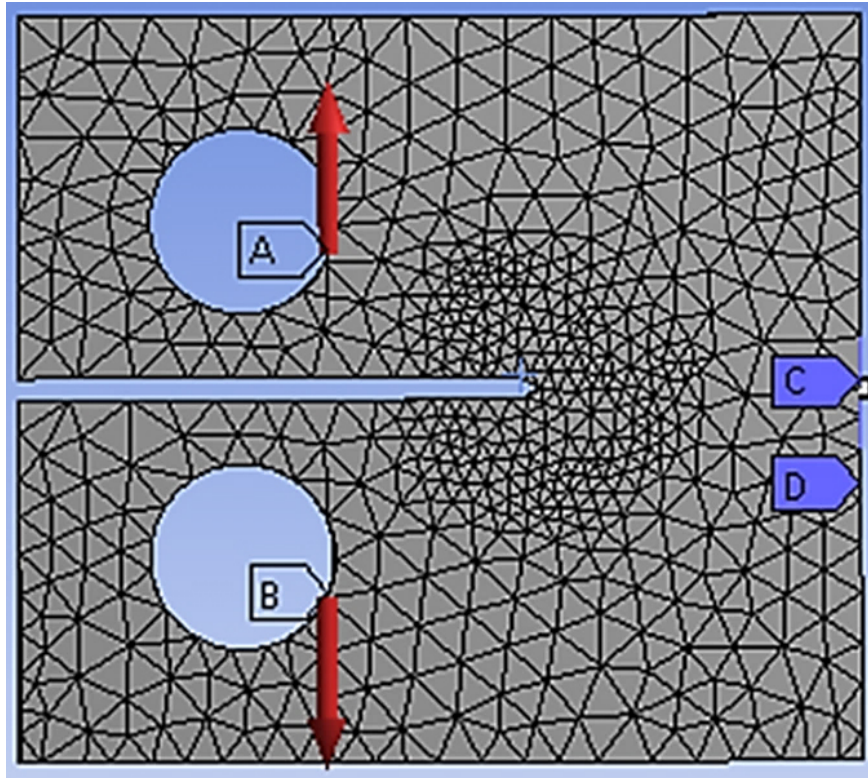


**Figure 7. Application of boundary conditions: opposing loads at A and B and displacement constraints at C and D.**

A methodology was proposed to analyze the stress intensity factor variation during crack growth, using three levels of constant loads,  $P$ . Initially, a gradually increasing load,  $P$ , ranging from zero to 48.0 kN, as shown in Fig. 8, was applied to determine the critical load,  $P_c = 32.4$  kN, responsible for initiating crack propagation. Fig. 9 illustrates the crack growth for the progressively ramping load, emphasizing the automatic mesh regeneration with crack advancement and the graphical solutions of the Von Mises stress field ( $\sigma$ ) from the simulations conducted in the Ansys program.

Subsequently, the concept was to apply constant loads exceeding the critical load  $P_c$  capable of propagating the crack, allowing the mapping the SIF evolution concerning the increase in crack length ( $K \times a$ ). The initial crack length was 20.0 mm, and the final length was 32.8 mm, which was defined for future comparison with experimental results. The crack growth analysis was divided into 13 smaller steps to ensure accuracy and convergence in the solution. The first step involved a linear solution, while the subsequent 12 steps were non-linear. Each step corresponded to an increment  $\Delta a$  in the crack length, allowing for the estimation of the number of cycles required for the crack to grow from an initial size  $a_i = 20.0$  mm to a final size  $a_f = 32.8$  mm. The numerical results were compared with experimental data obtained at a stress ratio  $R = 0.8$  for validation. A specific procedure was adopted to analyze the phenomenon. The crack was propagated under three levels of constant load:  $P_1 = 38.4$  kN,  $P_2 = 48.0$  kN, and  $P_3 = 55.0$  kN. For each step, the  $\Delta a$  increments and the values of the SIF during crack growth were calculated between  $a_i = 20.0$  mm and  $a_f = 32.8$  mm for all three loads. Subsequently,  $K \times P$  curves were established for the 13 solution steps at the three applied loads. Using the LR of these curves,  $K$  values were estimated for the experimental fatigue test loads,  $P_{min} = 4.0$  kN and  $P_{max} = 5.0$  kN with  $R = 0.8$ . From the LR equations,  $K_{min}$  and  $K_{max}$  values were calculated for the mentioned loads

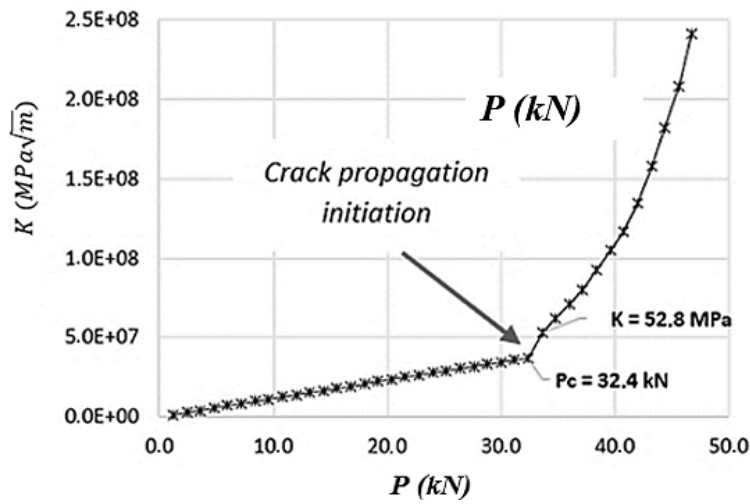


Figure 8. Numerical crack initiation model for critical load calculation  $P_c$ .

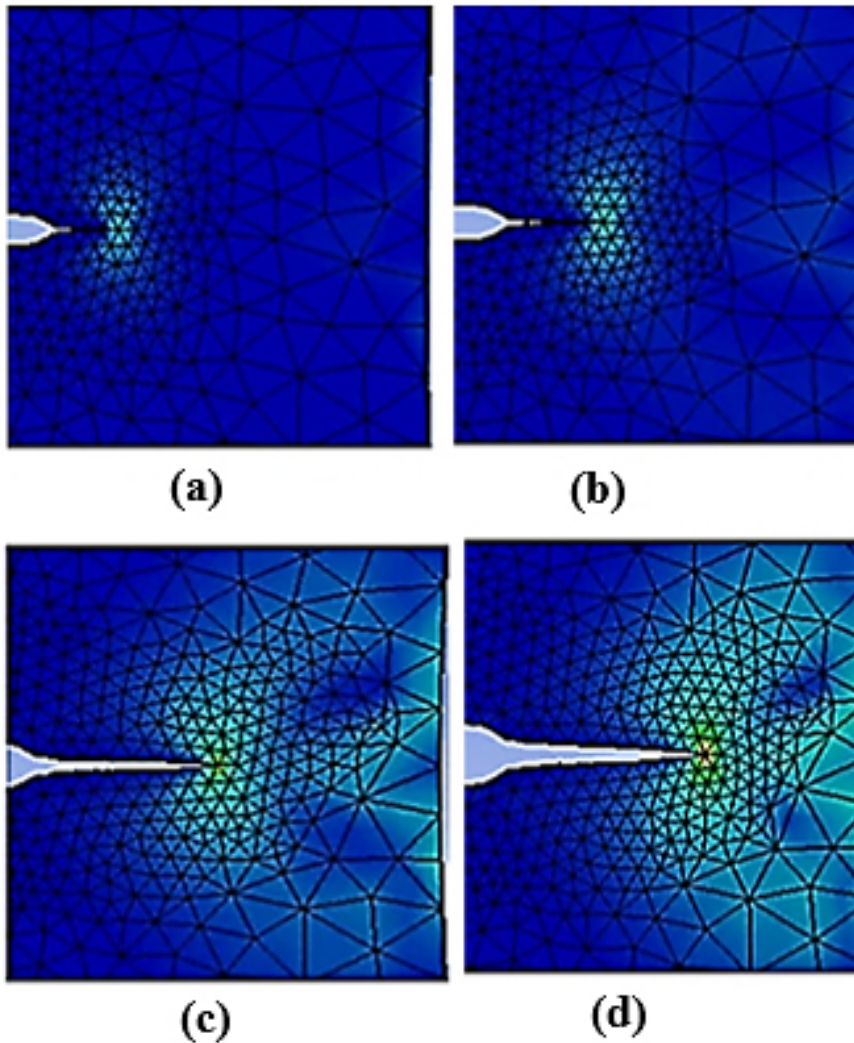


Figure 9. Crack growth for the gradually increasing ramped load and automatic mesh regeneration. a)  $P = 36.94$  kN,  $\sigma = 269.0$  MPa,  $K = 75.0$  MPa $\sqrt{m}$ ,  $a = 24.0$  mm; b)  $P = 39.4$  kN,  $\sigma = 310.0$  MPa,  $K = 95.0$  MPa $\sqrt{m}$ ,  $a = 26.5$  mm; c)  $P = 44.3$  kN,  $\sigma = 434.0$  MPa,  $K = 185.0$  MPa $\sqrt{m}$ ,  $a = 30.6$  mm; d)  $P = 46.8$  kN,  $\sigma = 522.0$  MPa,  $K = 241.0$  MPa $\sqrt{m}$ ,  $a = 32.0$  mm.

in all 13 steps.  $\Delta K$  values for use in the Paris equation and  $\Delta K'$  values for the Walker's equation were also determined. These equations calculated increase in the number of cycles in the Paris model  $\Delta N$  and increment in the number of cycles in the Walker's model  $\Delta N'$  values for each step. A  $\Delta a/\Delta N \times \Delta K$  finite element curve was developed and compared with the experimental  $da/dN \times \Delta K$  curve. Finally, the crack growth curves  $a \times N$  were compared using the Paris and Walker equations.

## RESULTS AND DISCUSSION

This work suggests that the procedure could be used in problems with standardized complex geometries after a numerical-experimental validation. The concept of similitude (Wang 1990, Anderson 2017), from fracture mechanics, can be applied in the solution, provided that the conditions at the crack tip are determined exclusively by a single loading parameter, such as the SIF. Therefore, two configurations would fail at the same critical value of  $K_c$  if an elastic singularity zone exists near the crack tip. In some instances of variable amplitude loading, especially with occasional overloads, the assumption of similitude may not be valid and other methods should be applied.

### Chemical analysis

The chemical composition in Table I shows that the values are within those specified by the SAE AMS 2355 standard (2002).

**Table I. Chemical analysis results (wt. %).**

Zn	Mg	Cu	Cr	Fe	Si	Ti	Al
5.79	1.95	1.76	0.24	0.07	0.05	0.05	Balance

### Monotonic properties

The results of tensile tests and fracture toughness for the aluminum alloy SAE AMS 7475-T7351 in the (L-T) orientation, along with the corresponding standard deviations ( $\delta$ ), are presented in Table II.

**Table II. Tensile and fracture toughness results.**

Orientation	UTS, MPa	$S_{ys}$ , MPa	RA,%	$\epsilon_v$ ,%	$K_{IC}$ , MPa $\sqrt{m}$
L-T	469(13.3)	395(13.0)	19(3.4)	16(1.2)	50.5(0.9)

Note: the numbers in parenthesis refer to  $\delta$  values; UTS, ultimate tensile strength;  $S_{ys}$ , yield strength;  $\epsilon_v$ , strain corresponding to tensile strength;  $K_{IC}$  is the Mode I plane strain fracture toughness; RA is reduction of area.

### Walker's model

For the Fatigue tests, Table III displays the results of the Paris coefficients  $C$  and the exponent  $m$  for the test specimens in the (L-T) orientation for various stress ratios  $R$ .

**Table III. Paris coefficient and exponent for (L-T) specimen orientations.**

Parameter	R=0.1	R=0.5	R=0.7	R=0.8
<i>m</i>	3.02	2.90	3.00	2.93
<i>C</i> (mm/cycle)	1.43E-7	3.17E-7	3.98E-7	4.21E-7

It was found that the Walker’s model successfully consolidated the fatigue crack propagation data from test specimens in the (L-T) orientation conducted for different applied stress ratios, *R*. In Fig. 10a, you can observe the *da/dN* x  $\Delta K$  curves without considering the effect of *R*, while in Fig. 10b, the curves generated with the Walker’s model take into account the impact of the stress ratio, *R*. The Walker’s model consolidated the fatigue crack propagation data at different applied stress ratios due to the low *R* dependence on exponent *m*.

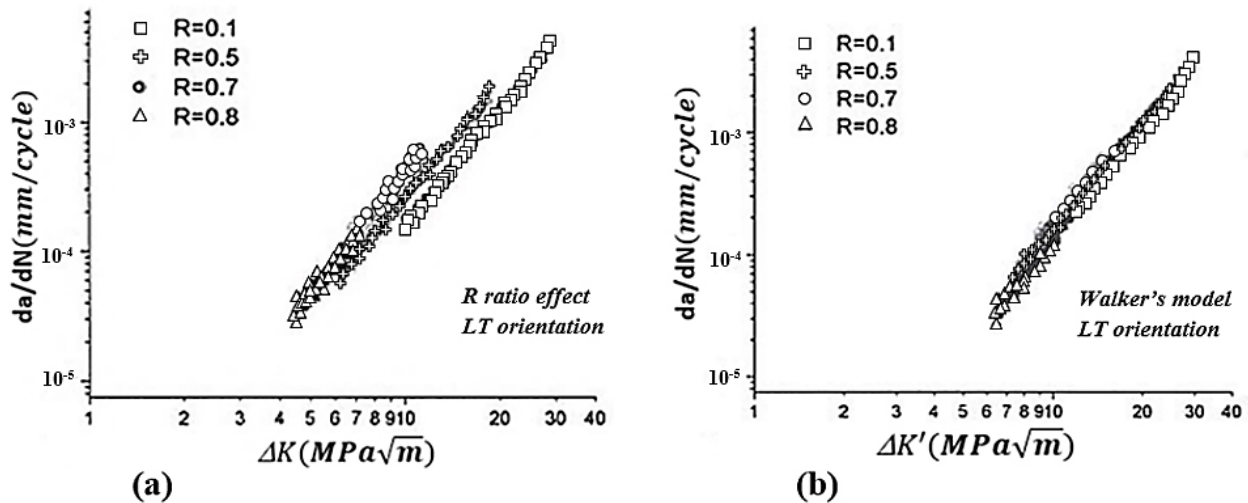


**Figure 10. Crack propagation curves for various R values in the (L-T) orientation for the SAE AMS 7475-T7351 aluminum alloy. a) Paris Model, b) Curves consolidated in the Walker’s Model.**

As a result, the Paris exponent, *m*, remains constant regardless of the stress ratio, *R*. Thus,  $m_0 = m$  and can be calculated by taking the average of the values at different *R* ratios. According to Table III, the average value of  $m = 2.96$ . To find the value of  $\gamma_w$ , a graph of  $\log C \times \log(1 - R)$  was first constructed, using the data from Table IV:

Through an LR of the curve, the coefficients of the equation were found as shown in Fig. 11. The coefficient of determination  $R^2$  was calculated and used to evaluate the quality of fit of the regression model ( $R^2 = 0.8627$ ).

$$\log C = -0.7118 (1 - R) - 6.809 \tag{10}$$

By comparing the coefficients of Eq. (10) with Eq. (4), it was possible to calculate  $\gamma_w$ . The term  $-(1 - \gamma_w)2.96 = -0.7118$ , therefore, the calculated value of  $\gamma_w$  from experimental data was indeed equal to 0.76.

**Table IV. Data for graph construction  $\log C \times \log(1 - R)$ .**

R	1 - R	C	logC	log(1 - R)
0.1	0.9	1.43E-07	-6.84466	-0.04576
0.5	0.5	3.17E-07	-6.49894	-0.30103
0.7	0.3	3.98E-07	-6.40012	-0.52288
0.8	0.2	4.21E-07	-6.37572	-0.69897

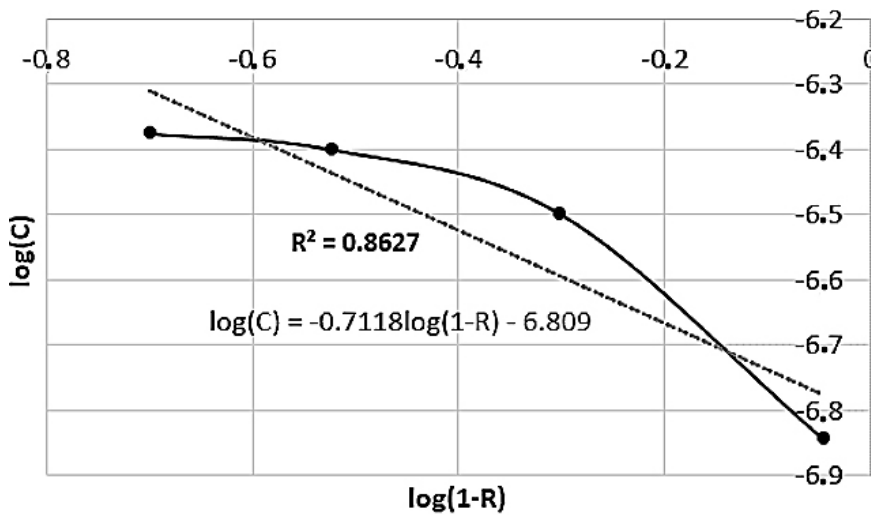


**Figure 11. Linear regression of the curve  $\log C \times \log(1 - R)$  for the calculation of  $\gamma_w$ .**

### Simulation results of stress intensity factor variation

The simulations allowed for observing of the stress intensity factor variation during crack growth under three constant load levels, enabling the generation of curves that depict the evolution of SIF as a function of crack growth ( $K \times a$ ), as illustrated in Fig. 12.

### Linear regression of the stress intensity factor

The main objective of LR is to identify the most suitable equation for predicting the value of SIF based on input values of  $P$ . It is important to note that  $K$  is a variable of interest and is being estimated based on the applied loads  $P$ . The relationship between  $K$  and  $P$  is linear. On the other hand, the variation of  $K$  with crack growth  $a$  is nonlinear. This nonlinearity of  $K$  does not influence the linear regression process, as in this procedure, the crack size value is considered constant. In Fig. 13, the  $K \times P$  curves are presented to estimate  $K$  values through LR for the loads  $P_{min} = 4.0$  kN and  $P_{max} = 5.0$  kN.  $K \times P$  curves for the 13 steps (different crack lengths) for loads  $P_1, P_2,$  and  $P_3$  are shown. The equations for estimating SIF obtained through LR are presented in Table V. The  $\Delta K'$  values are obtained after correcting the numerically calculated  $\Delta K$  by multiplying it by the factor  $(1 - R)^{-(1-\gamma_w)}$  obtained experimentally.

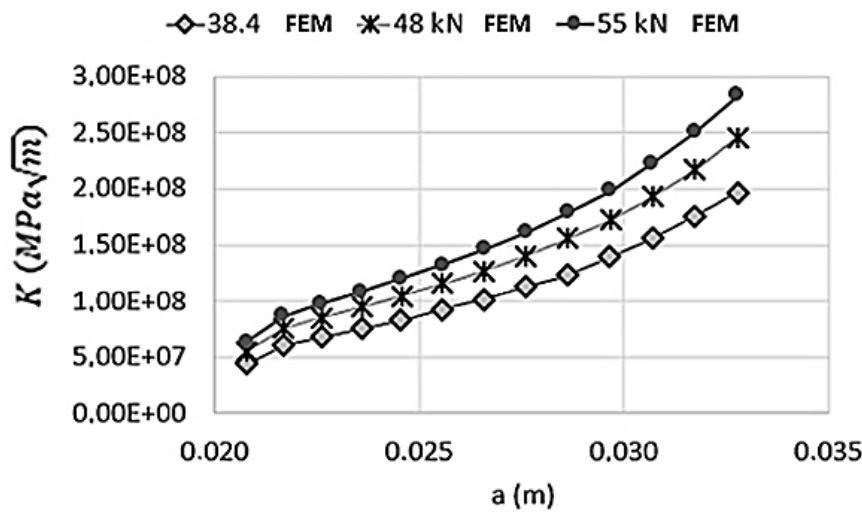


Figure 12. Curves of the variation of K with increasing crack size (K x a) using the FEM.

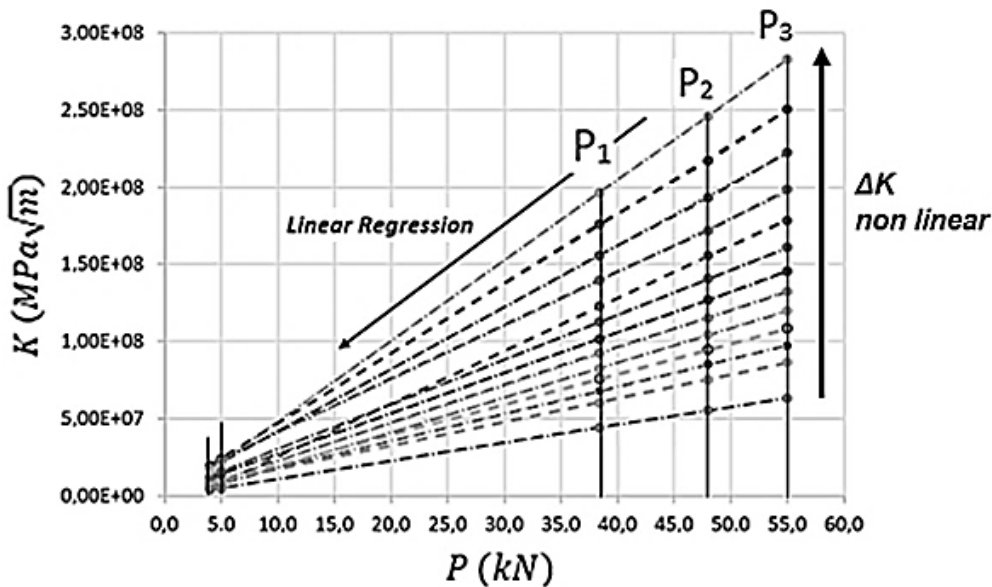
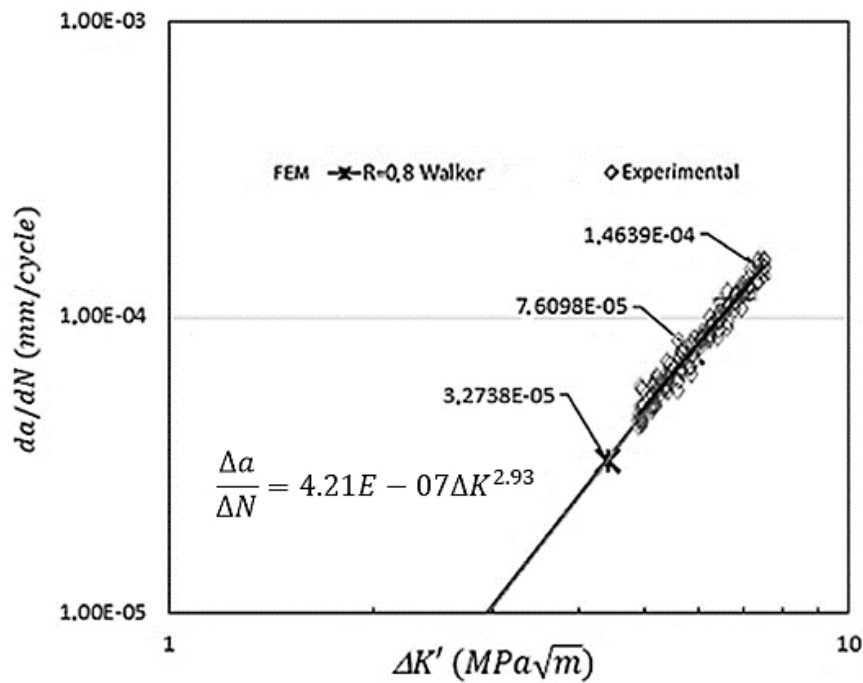


Figure 13. Estimating of SIF values for the loads  $P_{min} = 4.0$  kN and  $P_{max} = 5.0$  kN by linear regression of the SIF calculated at each simulation stage for the loadings  $P_1$ ,  $P_2$ , and  $P_3$ . It's important to note that the variation of K with the crack growth is nonlinear. On the other hand, the variation of K for the same crack length is linear.

The Fig. 14 displays the results of FEM simulation for the  $da/dN \times \Delta K'$  curve, comparing them with experimental results. Both utilized the Walker's model with an exponent  $\gamma_w = 0.76$  and stress ratio  $R = 0.8$ . It was observed that the numerical results adequately represented the experimental results, confirming the numerical validation of the model.

To compare the effectiveness of the Paris and Walker's models for life prediction, Fig. 15 presents the FEM simulation results of crack growth curves,  $a \times N$ . The first curve uses the Walker's model, and the second uses the Paris model; the latter does not consider the effect of the stress ratio  $R$ . Without considering the impact of the load ratio  $R$ , the results showed that life estimation through



**Figure 14.** Results of FEM simulation and experimental data for the  $da/dN \times \Delta K'$  curve using the Walker's model ( $\gamma_w = 0.76$ ) and stress ratio  $R = 0.8$  for the SAE AMS 7475-T7351 aluminum alloy.

**Table V.** Equations for estimating K obtained through linear regression of the SIF.

Step	$a(mm)$	$\Delta a(mm)$	Equations	$\Delta K'$ MPa $\sqrt{m}$	$\Delta N$ (cycles) (Paris)	$\Delta N'$ (cycles) (Walker)
0	20.0	-	-	-	-	-
1	20.8	0.8	$K = 2E+06P + 627.95$	1.47	1874561	604016
2	21.7	1.7	$K = 2E+06P - 627183$	2.94	276728	89167
3	22.6	2.6	$K = 2E+06P + 12931$	2.94	291820	94030
4	23.6	3.6	$K = 2E+06P - 3E+06$	2.94	301687	97209
5	24.6	4.6	$K = 2E+06P + 561788$	2.94	306418	98733
6	25.6	5.6	$K = 3E+06P - 696440$	2.94	312549	100709
7	26.6	6.6	$K = 3E+06P + 902966$	4.41	95850	30885
8	27.6	7.6	$K = 3E+06P - 7E+06$	4.41	97462	31404
9	28.6	8.6	$K = 4E+06P + 4E+06$	4.41	97490	31413
10	29.6	9.7	$K = 4E+06P + 2E+06$	5.89	41819	13475
11	30.7	10.7	$K = 4E+06P + 4E+06$	5.89	42051	13550
12	31.7	11.7	$K = 5E+06P - 3E+06$	5.89	42088	13561
13	32.8	12.8	$K = 5E+06P - 3E+06$	7.36	22048	7104

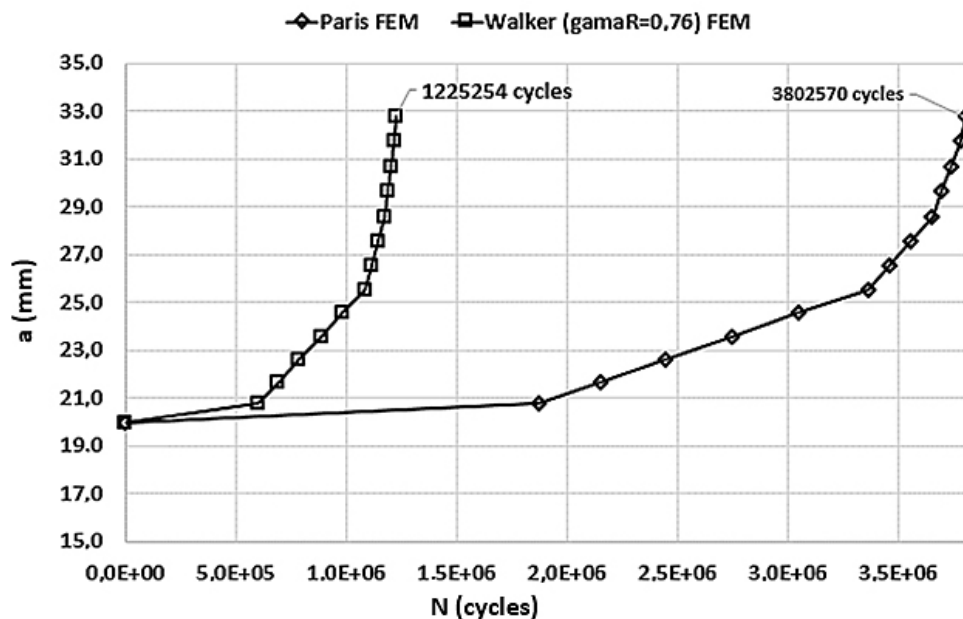


**Figure 15.** Results of FEM simulation for crack growth curves,  $a \times N$ . The first curve uses the Walker's model with  $R=0.8$  and  $\gamma_w=0.76$ , and the second uses the Paris model.

the integration of the Paris equation, becomes very conservative and is not suitable for life prediction. The number of cycles using the Paris model ( $\Delta N/\Delta N'$ ) was 3.1 times greater than in the Walker's model.

## CONCLUSIONS

The objective of this study was to introduce an original numerical-experimental procedure for analyzing crack growth in SAE AMS 7475-T7351 aluminum alloy subjected to longitudinal loading in the L-T rolling orientation. This innovative approach, developed by the authors, integrates Walker's model and the Finite Element Method (FEM) to investigate the influence of stress ratio on  $da/dN$  data. Combining the finite element method with linear regression of the stress intensity factor (SIF), the numerical SIF results were aligned with Walker's model, incorporating the effect of stress ratio  $R$ , using experimental data obtained from constant amplitude loads with a stress ratio of  $R = 0.8$ . The developed numerical-experimental procedure, integrating Walker's approach, FEM, and LR of SIF, demonstrated effectiveness in representing experimental data. Comparative analysis of life prediction models revealed that Walker's model, incorporating the effect of stress ratio  $R$ , outperformed the Paris-Erdogan model, resulting in less conservative life estimates. Based on literature and applying concepts of similitude in fracture mechanics, the numerical validation of the model indicates that this methodology can accurately predict fatigue life in scenarios with complex geometries, where calculating the fracture parameter  $K$  is challenging, and the finite element method proves effective.

## Acknowledgments

Thanks to the Department of Geosciences and Engineering of the Federal University of the South and Southeast of Pará for providing access to the Finite Element Code ANSYS used in this work and EMBRAER-Brazil for providing the materials used in this research.

## REFERENCES

- ANDERSON TL. 2017. Fracture Mechanics: fundamentals and applications. 4th ed. Boca Raton: CRC Press Taylor and Francis Group, 688 p.
- ANSYS. 2015. ANSYS mechanical APDL technology demonstration guide - Release 16.
- BANNANTINE J, CORNER J & HANDROCK J. 1990. Fundamentals of metal fatigue analysis. Research supported by the University of Illinois. Englewood Cliffs, New Jersey: Prentice Hall, 286 p.
- BILBY B, COTTRELL A & SWINDEN K. 1963. The spread of plastic yield from a notch. Proceedings of the Royal Society of London Series A Math Phys Sci 272(1350): 304-314.
- CHANG J & HUDSON C. 1981. Methods and models for predicting fatigue crack growth under random loading. 748. ASTM International.
- CHEMIN A. 2012. Avaliação da propagação de trinca associada à corrosão da liga 7475 T7351 submetida a carregamentos de voos simulados. Ph.D. thesis. Programa de Pós-Graduação em Engenharia Mecânica e Área de Concentração em Materiais – Escola de Engenharia de São Carlos da Universidade de São Paulo. URL <http://www.teses.usp.br/teses/disponiveis/18/18150/tde-14112012-183154/>. Dissertação (Mestrado). Unpublished.
- COURTIN S, GARDIN C, BÉZINE G & HAMOUDA H. 2005. Advantages of the J-integral approach for calculating stress intensity factors when using the commercial finite element software ABAQUS. Eng Fract Mech 72(14): 2174-2185.
- DATTA S, CHATTOPADHYAY A, IYER N & PHAN N. 2018. Fatigue crack propagation under biaxial fatigue loading with single overloads. Int J Fatigue 109: 103-113.
- DECOOPMAN X. 1999. Influence des conditions de chargement sur le retard a' la propagation d'une fissure de fatigue apre's l'application d'une surcharge. Ph.D. thesis. Université de Sciences et Technologies de Lille. doi:<https://doi.org/10.1016/j.ijfatigue.2007.02.002>. Tese (Doutorado).
- DURAN J & HERNANDEZ C. 2015. Evaluation of three current methods for including the mean stress effect in fatigue crack growth rate prediction. Fatigue Frac Eng Mater Struct 38(4): 410-419.
- ELBER W. 1971. The significance of fatigue crack closure. ASTM STP 2(4): 230-242.
- FORMAN R, KEARNEY V & ENGLE R. 1967. Numerical analysis of crack propagation in cyclic-loaded structures. J Basic Eng 89: 459-464.
- FORMAN R & METTU S. 1992. Behavior of Surface and Corner Cracks Subjected to Tensile and Bending Loads in Ti-6Al-4V Alloy. Vol. 1. American Society for Testing and Materials, 519-546 p.
- GALIC I, CULAR I, VUCKOVIC K & TONKOVIĆ Z. 2018. Comparison of SIF solutions obtained by XFEM and conventional FEM for cracks in complex geometries like valve body. Procedia Struct Integrity 13: 2109-2113.
- LAZZERI L, PIERACCI A & SALVETTI A. 1995. An evaluation of fatigue crack growth prediction methods used in aircraft design. Proceeding of ICAF 95.
- MILLER M & GALLAGHER J. 1981. An analysis of several fatigue crack growth rate (FCGR) descriptions. ASTM STP 738: 205-251.
- MONTEZUMA M. 2022. Simulação do efeito de retardo e aceleração de propagação de trincas para previsão de vida à fadiga de ligas de alumínio 2050-t84 e 7475-t7351 de grau aeronáutico. Ph.D. thesis. Universidade federal do Ceará, Centro de tecnologia, Programa de Pós-Graduação em Engenharia e Ciência de Materiais. Fortaleza. URL <http://repositorio.ufc.br/handle/riufc/70133>. Tese (doutorado).
- NARNE J, SANDHYA V, YERRAMSETTY N & REDDY V. 2018. Experimental and Numerical Investigations on Crack Propagation in Titanium Alloys. Int J Curr Eng Technol 8(4): 922-927.
- NEWMAN J. 1998. The merging of fatigue and fracture mechanics concepts: a historical perspective. Prog Aerosp Sci 34(5-6): 347-390.
- OGURA K, MIYOSHI Y & NISHIKAWA I. 1985. Fatigue crack growth and closure of small cracks at the notch root. Current Research on Fatigue Cracks (A 86-33002 14-39). Society of Materials Science, p. 57-78.
- PARIS P, GOMEZ M & ANDERSON W. 1961. A rational analytical theory of fatigue. Trend Eng 13: 9-14.
- RICE J. 1968. A path-independent integral and the approximate analysis of strain concentration by notches and cracks. J Appl Mech 35(2): 379-386.
- ROSENFELD A. 1997. Fracture Mechanics in Failure Analysis, Metals Handbook: Fatigue and Fracture. Vol. 19. Tenth ed. ASM International, 450-456 p.
- RUCHERT C. 2007. Estudo da inferência de carregamento em histórias de voos simulados na liga de Al aeronáutico SAE-AMS 7475 T7351. Ph.D. thesis. Ciência e Engenharia de Materiais, Universidade de São Paulo. São Carlos. URL <https://doi.org/10.11606/T.88.2007.tde-22092008-131854>. Tese (Doutorado em Ciência e Engenharia de Materiais).
- SAE AMS 2355. 2002. Quality Assurance Sampling and Testing of Aluminum Alloys and Magnesium Alloys, Wrought Products, Except Forging Stock, and Rolled, Forged, Or Flash Welded Rings. Aer Mat Spec SAE Int.

SONG S & PAULINO G. 2006. Dynamic stress intensity factors for homogeneous and smoothly heterogeneous materials using the interaction integral method. *Int J Solids Struct* 43(16): 4830-4866.

TODARO E, RÜCHERT C, MILAN M, BOSE FW, TARPANI J & SPINELLI D. 2006. Modeling of Stress Ratio Effect on Al Alloy SAE AMS 7475-T7351: Influence of Loading Direction. *J Mater Eng Perform* 15(5): 608-613.

TOMKINS B. 1968. Fatigue crack propagation – an analysis. *Philos Mag* 18(155): 1041-1066.

TONG DEA. 2019. Prediction of crack growth life 2A97-T3 lithium aluminum alloy under Mini-Twist load spectrum. In: IOP Conference Series: Materials Science and Engineering, Vol. 490, p. 022006. IOP Publishing.

WALKER K. 1970. The Effect of Stress Ratio During Crack Propagation and Fatigue for 2024-T3 and 7075-T6 Aluminum, Effects of Environment and Complex Load History on Fatigue Life. *ASTM STP* 462: 1-14.

WANG C. 1990. An improvement of applying similarity methods to fracture mechanics-measurement of fractures toughness  $K_{Ic}$ ,  $k_q$  values by small-scale single specimen. *Eng Fract Mech* 36(2): 313-320.

WILLIAMS M. 1957. On the stress distribution at the base of a stationary crack. *J Appl Mech* 24(1): 109-114.

YANG T. 1986. Finite element structural analysis. New Jersey, USA: Prentice-Hall, Inc, 543 p.

YAU J, WANG S & CORTEN H. 1980. A mixed mode crack analysis of isotropic solids using conservation laws of elasticity. *J Appl Mech* 47(2): 335-341.

ZHENG J & POWELL B. 1999. Effect of Stress Ratio and Test Methods on Fatigue Crack Growth Rate for Nickel Based Superalloy Udimet720. *Int J Fat* 21(5): 507-513.

ZIENKIEWICZ O. 1994. The finite element method. V.1. Basic Formulation and Linear Problems. McGraw-Hill International, 648 p.

#### How to cite

MONTEZUMA MFV, DE DEUS EP, RÜCHERT COFT, CARVALHO MC & SILVA FILHO MA. 2024. Numerical-experimental procedure for predicting fatigue life in SAE AMS 7475-T7351 aluminum alloy considering the effect of stress ratio. *An Acad Bras Cienc* 96: e20231400. DOI 10.1590/0001-3765202420231400.

*Manuscript received on December 28, 2023;  
accepted for publication on May 26, 2024*

#### MARCOS FÁBIO V. MONTEZUMA<sup>1</sup>

<https://orcid.org/0000-0002-8669-0422>

#### ENIO P. DE DEUS<sup>2</sup>

<https://orcid.org/0000-0002-3933-0803>

#### CASSIUS OLIVIO F.T. RÜCHERT<sup>3</sup>

<https://orcid.org/0000-0002-9912-0250>

#### MÁRCIO C. DE CARVALHO<sup>4</sup>

<https://orcid.org/0000-0001-9162-2363>

#### MARCELO A. E SILVA FILHO<sup>5</sup>

<https://orcid.org/0000-0003-0396-8482>

<sup>1</sup>Vibra Energia S.A., Rua Correia Vasques, 250, 20211-140 Rio de Janeiro, RJ, Brazil

<sup>2</sup>Universidade Federal do Ceará, Departamento de Engenharia Metalúrgica e de Materiais, Av. Mister Hull, s/n, Pici, 60455-760 Fortaleza, CE, Brazil

<sup>3</sup>Universidade de São Paulo, Departamento de Engenharia de Materiais, Estrada Municipal Chiquito de Aquino, 1000, Mondesir, 12612-550 Lorena, SP, Brazil

<sup>4</sup>Universidade Federal do Sul e Sudeste do Pará, Escola de Engenharia de Materiais, Folha 17, Quadra 04, Lote Especial - Nova Marabá, 68505-080 Marabá, PA, Brazil

<sup>5</sup>Universidade Federal do Ceará, Campus do Pici, Departamento de Computação, Av. Mister Hull, s/n, Pici, 60455-760 Fortaleza, CE, Brazil 60020-181 Fortaleza, CE, Brasil

Correspondence to: **Marcos Fábio V. Montezuma**

E-mail: [mfabiomontezuma@gmail.com](mailto:mfabiomontezuma@gmail.com)

#### Author contributions

MARCOS FÁBIO V. MONTEZUMA: Conceptualization, Methodology, Formal analysis, Writing and Original Draft. ENIO P. DE DEUS: Validation, Supervision. CASSIUS OLIVIO F.T. RÜCHERT: Investigation, Validation, Supervision. MÁRCIO C. DE CARVALHO: Writing, Review & Editing, Validation. MARCELO A. E SILVA FILHO: Software, Validation.

